

Published in final edited form as:

Analyst. 2019 November 07; 144(21): 6240–6246. doi:10.1039/c9an01137d.

Tunable Optical Metamaterial-Based Sensors Enabled by Closed Bipolar Electrochemistry

Garrison M. Crouch¹, Christiana Oh¹, Kaiyu Fu², Paul W. Bohn^{1,2,*}

¹Department of Chemical and Biomolecular Engineering, University of Notre Dame, Notre Dame, IN 46556

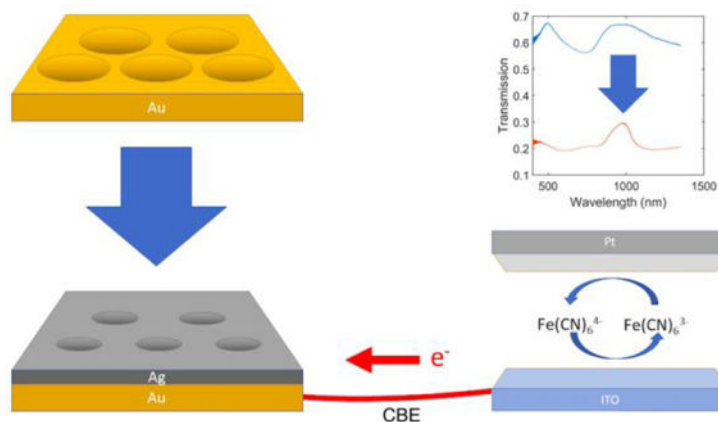
²Department of Chemistry and Biochemistry, University of Notre Dame, Notre Dame, IN 46556

Abstract

Enabled by the proliferation of nanoscale fabrication techniques required to create spatially-repeating, sub-wavelength structures to manipulate the behavior of visible-wavelength radiation, optical metamaterials are of increasing interest. Here we develop and characterize a chemical sensing approach based on electrochemical tuning of the optical response function of large-area, inexpensive nanoaperture metamaterials at visible and near-IR wavelengths. Nanosphere lithography is used to create an ordered array of sub-wavelength apertures in a Au film. The spacing of these apertures is established during fabrication, based on the size of the polystyrene nanospheres. Tunable shifts in the transmission spectrum can be produced post-fabrication by electrodeposition of a dissimilar metal, Ag, using the nanoaperture film as one electrode in a 2-electrode closed bipolar electrochemical (CBE) cell, altering hole size, film thickness, and film composition while maintaining hole spacing dictated by the original pattern. Optical transmission spectra acquired under galvanostatic conditions can be expressed as a linear combination of the initial and final (saturated) spectra, and the resulting response function exhibits a sigmoidal response with respect to the amount of charge (or metal) deposited. This architecture is then used to perform optical coulometry of model analytes in a CBE-based analyte-reporter dual cell device, thus expanding the capability of CBE-based sensors. Increasing the exposed electrode area of the analyte cell increases the response of the device, while modifying the circuit resistance alters the balance between sensitivity and dynamic range. These tunable nanoaperture metamaterials exhibit enhanced sensitivity compared to CBE electrochromic reporter cells to the μM to nM concentration range, suggesting further avenues for development of CBE-based chemical sensors as well as application to inexpensive, point-of-care diagnostic devices.

Graphical Abstract

* Author to whom correspondence should be addressed, pbohn@nd.edu, Tel.: +1 574 631 1849; Fax: +1 574 631 8366.



Summary Statement

Closed bipolar electrochemistry to couple an analytical reaction to an optical readout by the reconfiguration of an optical metamaterial.

Introduction

Improved sensitivities and fast response times have followed developments in functional biomaterials, and advances in fabrication have yielded biosensors in which biomolecular and electronic components are integrated.^{1–4} Electrochemical biosensors, in particular, frequently combine a bio-recognition element with electrochemical transduction.^{5, 6} In this regard, there is great interest in pursuing novel methods of reading out the bio-recognition event, and nature suggests a novel route to do so. For example, the brilliantly iridescent wing of the Morphinae butterfly is a well-known natural example of an optical metamaterial – a nanostructured material that exploits repetitive interactions of light to create structural color from a colorless bulk material - in the case of the butterfly, a striking blue that does not fade with time or exposure to light.⁷

Materials which utilize subwavelength structures to direct the propagation of electromagnetic radiation, in ways not available to bulk materials, are the subject of intense current research⁸ due to exciting capabilities presented by non-classical optical phenomena, *e.g.* negative refractive index materials for cloaking.⁹ A particularly accessible category of subwavelength metamaterial structures is based on spatially repeating nanoapertures, which can access a wide range of optical properties depending on the hole size, spacing, geometry, and metallic film thickness.¹⁰ For example, single, or distantly-spaced, nanoapertures, may exhibit zero-mode waveguide behavior and block propagating modes of light, a property which has been used for single-molecule fluorescence studies.¹¹ In larger, more closely-spaced arrays, nanoaperture-based metamaterials may exhibit extraordinary optical transmission,¹² useful in applications including bandpass optical filters¹³ and direct chemical sensing.¹⁴ A particularly appealing top-down, massively-parallel fabrication strategy to achieve these closely-spaced arrays is based on nanosphere lithography (NSL) - first developed for producing nanopillar arrays¹⁵ and then later extended to nanoaperture arrays by adding an etch step.^{16, 17}

The work described here exploits the characteristic optical response function of nanoaperture-based metamaterials to achieve electrochemically-tunable electrochromic behavior for chemical sensing. The spectral changes of nanoaperture metamaterials is not due to a change in the underlying electronic structure. Instead, the morphology of the architecture is altered through the electrodeposition of a dissimilar metal, thus altering the size of the holes in the array and the nature of the composite metallic architecture. This is philosophically similar, yet nearly opposite in implementation, to the approach recently demonstrated by Wang and Chu, *et. al.*,¹⁸ in which a tunable metamaterial was realized *via* electrodeposition of silver onto gold nanodots.

In this work, we utilize closed bipolar electrochemistry (CBE) - an effective method to exploit the unique properties of non-powered, electrified interfaces.¹⁹⁻²² Prior work from our laboratory^{23, 24} established a two-cell CBE device, in which the analyte-targeted redox reaction (analyte cell) was physically separated from the readout mechanism (reporter cell). In the first version of the device, the reporter cell employed a readout based on the electrochromic reduction of colorless methyl viologen dication, MV^{2+} , to its purple, radical cation, $MV^{+\bullet}$. In the present work, we develop a new concept for sensor readout by replacing the electrochromic reaction with a NSL-fabricated nanoaperture metal metamaterial, the transmission spectrum of which is then altered by electrodeposition or electrodisolution of Ag, thereby effecting structure-based color changes. Since the change in the transmission spectrum is a function of the amount of Ag deposited, the nanoaperture array can be used to correlate the magnitude of the optical readout to the amount of charge transferred, thus translating coulometric efficiency of the analytical reaction to a measurable shift in the optical transmission spectrum. Both the transmission spectrum as well as the maximum transmitted intensity change may be described by a sigmoidal sensor-response curve. Proof-of-principle for this sensing scheme is demonstrated by using nanoapertured Au to detect $Fe(CN)_6^{4-}$ down to 10 μM in standard cells, extending to 10 nM with special cell design and series resistance to control the rate of charge transfer.

Experimental Section

Metamaterial Fabrication and Characterization.

NSL was used to create nanoapertured metamaterials with different hole sizes and spacings to tune the optical response. Polystyrene beads in aqueous solution with mean diameter of 0.6 μm were obtained from Sigma-Aldrich and used as received. Beads were mixed 1:1 in ethanol, then pipetted into a glass dish filled with DI water ($\rho \sim 18.2 M\Omega cm$, Millipore) to form a self-assembled monolayer.²³ Glass slides (Schott) were treated in O_2 plasma prior to immersion in the solution. After transfer of the monolayer onto the glass, beads were etched via O_2 plasma (Plasma Therm 790 RIE) and 50 nm Au with 5 nm Ti was deposited by e-beam evaporation (Oerlikon.) Transmission measurements were performed, as shown in Figure S1 (Supplemental Information, SI), using a fiber-coupled, stabilized tungsten lamp (ThorLabs, SLS202L) which was expanded and passed through neutral density filters before being focused on the sample. The sample was placed at the focal plane of the illumination path, with transmitted light collected and coupled into a multi-mode optical fiber from which it was directed into a grating spectrometer (Princeton Instruments, Acton SpectraPro

SP-2750) fitted with a PyLoN cryogenically-cooled CCD camera. Spectra were acquired in LightField and imported into Matlab (2018b) for further processing.

Electrodeposition.

Polyvinyl butyral (PVB), copper (II) chloride, tetrabutylammonium bromide (TBABr), silver nitrate (AgNO_3), and dimethyl sulfoxide (DMSO) were ordered from Sigma-Aldrich and used as received. The electrodeposition solution was designed after a composition previously reported to produce optically-reflective Ag films,²⁵ but with CuCl_2 , AgNO_3 , and TBABr concentrations increased to decrease the overpotential required to yield practical deposition rates. Solutions used in these experiments were 12 mM AgNO_3 , 2.4 mM CuCl_2 , and 50 mM TBABr with 10 wt% PVB in DMSO. Electrodeposition was controlled with a Gamry Reference 600 potentiostat in a 2-electrode configuration with an ITO-coated glass slide as the quasi-reference/counter electrode (QRCE).

Analyte and Reporter Cell and CBE Configuration.

Sensor devices were constructed with separate analyte and reporter cells connected by a CBE, as shown schematically in Figure S1(a). The analyte cell was constructed using a standard glass slide (VWR) coated with Ti/Pt (10 nm/100 nm), a tape spacer (50 μm , Scotch), and an ITO-coated glass slide (Sigma, 8–12 Ω/sq). A 4 mm hole punched in the tape spacer created the containment volume for the analyte solution, which was overfilled (10 μL) prior to assembly. Potassium ferrocyanide ($\text{Fe}(\text{CN})_6^{4-}$) (Fisher Scientific) was used as received and dissolved in deionized water (18.2 M Ω cm, Millipore) with 0.1 M KCl supporting electrolyte (Sigma Aldrich). The reporter cell consisted of the nanoaperture metamaterial, as described above, along with two glass microscope slide spacers (Schott), and an ITO-coated glass slide, with Teflon tape (Uline) to prevent leakage. Holes of diameters *ca.* 4 mm and 6 mm, were drilled in spacers 1 and 2, respectively, with a channel milled in spacer 2 to allow injection of the electrodeposition solution *via* syringe after device assembly. Cells were clamped with sufficient pressure to prevent leakage. *In situ* optical measurements of the reporter cell were performed in a custom measurement apparatus, shown in Figure S1(b), using transmission reference spectra acquired with a bare glass slide, instead of the nanoaperture metamaterial. The Pt-coated glass slide of the analyte cell was used as the working electrode, with the ITO slide of the reporter cell as the QRCE. An insulated Al-core wire was affixed to the nanoaperture material of the reporter cell and the ITO slide of the analytical cell to create the CBE.

Results and Discussion

Optical Response of Nanoapertured Metamaterials.

NSL is a facile method for producing large-area, well-ordered nanoaperture arrays for electrochemical and optical applications.²⁶ Aperture spacing and size may be manipulated by changing the size of nanospheres used to template the array and the O_2 plasma etch time, respectively. Prior to O_2 plasma etching, removal of the polystyrene spheres yielded a film consisting of discontinuous trigonal nanopyramids.²⁷ To examine the change in optical transmission as a function of nanoaperture size while maintaining aperture spacing, the O_2 plasma etch time was varied in more granular steps, with transmission spectra taken after the

initial onset of film conductivity (30 s etch time) as shown in Figure 1. First, an overall decrease in transmission is observed with decreasing aperture size, which is reasonable given the increasing proportion of metal to clear aperture area. Aperture areas measured by plan view SEM and analyzed with ImageJ are plotted in Figure S2 and show that the radii of nanoapertures arrays can be tuned from 287 nm to 227 nm for etch times from 40 s to 2 min, respectively. These limits were selected consistent with the onset of film conductivity at ~30 s etch time. At etch times exceeding 2 min, the beads used for NSL templating were damaged and difficult to remove. The peak in transmission near 500 nm, Figure 1(a), is attributed to bulk Au,²⁸ while the gradual transition from a relatively flat response at wavelengths >600 nm to a distinct peak centered at ~1000 nm is attributed to the evolution of nanoaperture structure, as are less pronounced peaks at *ca.* 700 nm and 1625 nm. Because all of these transmission peaks are at wavelengths greater than twice the diameter of the apertures in the metamaterial, shifts in these peaks are attributed to differences in nanoaperture structure.²⁸

Post-Fabrication Tunability.

The ability to tune the nanoaperture metamaterial structure post-fabrication is critical to the proposed mechanism for optical coulometry in the assembled CBE device. The effect of metal electrodeposition onto an idealized nanoaperture array was simulated using a 3-dimensional finite-element simulation (COMSOL) - required due to the hexagonal lattice structure. In this simulation, a complete unit cell was modeled using a 50 nm Au film at the glass-air interface with 580 nm diameter apertures on a 600 nm pitch hexagonal lattice and with Floquet periodicity at the boundaries. Transmission was computed for each frequency and, as shown in Figure S3, the calculated transmission spectrum transitions from relatively flat in the infrared with 5 nm of Ag to exhibit a well-defined peak at ~850 nm with increasing Ag thickness, the emergent near-IR peak at ~850 nm being a key feature which was selected for experimental study.

To experimentally characterize the kinetics of the optical changes, a reporter cell was assembled with the nanoaperture metamaterial connected to the potentiostat as the working electrode, with the ITO slide acting as a QRCE. An initial blank transmission spectrum was acquired with a glass slide of the same type as the nanoaperture metamaterial substrate. In addition, an initial spectrum with an as-fabricated nanoaperture metamaterial was acquired to establish a $t = 0$, $Q = 0$ baseline before any charge, Q , was passed. Galvanostatic conditions were then established with 20 μ A current applied for specified increments up to a maximum of 300 s. After each application, a transmission spectrum was acquired, as shown in Figure 2(a). Figures 2(b) and 2(c) demonstrate the reduction in nanoaperture radius before and after Ag deposition. Comparing these spectra to the simulation results in Figure S3, the experimental spectra show the same general spectral bands and trends with thickness, although broader and red-shifted. The broadening of the experimental peaks is likely due to fabrication nonidealities, as literature suggests that parameters such as metal film roughness,²⁹ scattering from metal and dielectric imperfections,³⁰ and slight hole size differences³¹ are causes of resonance peak broadening. Also of note are the gradual disappearance of the peak at 500 nm (attributed to bulk Au), indicating that electrodeposited Ag gradually covers the Au NSL-derived template with thicknesses approaching the 40–60 nm, as well as a redshift

of the near-IR peak at *ca.* 900 nm. The total experimental red-shift is estimated to be $\lambda \sim 41$ nm, while the simulations give $\lambda \sim 36$ nm (from 60 nm to 100 nm Ag). This observation is consistent with the growth of the Ag intensity in the energy-dispersive x-ray (EDX) images given in Figures S3 and S4, acquired before and after Ag deposition. The main result of both simulations and experiments is that the near-IR feature identified in Figures 2 and S2 becomes more pronounced with increasing Ag deposition.

To obtain a metric for sensor response, the transmission spectra were first normalized to unit area to account for the decrease in transmission with increasing Ag deposition, the result being termed the intensity response. Each normalized spectrum was then fit to a linear combination of the starting ($t = 0$ s, S_0) and ending ($t = 300$ s, S_{300}) spectra, with a single variable, x , governing the relative weighting, *i.e.*

$$S(t) = xS_{300} + (1 - x)S_0 \quad (1)$$

Plotting this variable against the cumulative deposition time in a galvanostatic experiment, as shown in Figure 3, yields a sigmoidal sensor-response curve.³² The charge transferred from analytical to reporter cell, Q , can be calculated from the galvanostatic current, i , and the deposition time t_{dep} as:

$$Q = \int_0^t i dt = 20 \mu A * t_{dep} \quad (2)$$

Because the current is constant in a galvanostatic experiment, we conclude that the sensor exhibits a large response range from 0 to 6 mC (*i.e.* $t = 0$ to 300 s). Similarly, the overall change in intensity of each spectrum can be plotted *vs.* deposition time, which produces a similar sigmoidal response curve. A sigmoidal curve was fit to the average of the two response metrics to define an overall sensor response, SR:

$$SR = \left(\frac{A}{1 + e^{-B * (Q - C)}} + D \right) \quad (3)$$

where Q is the charge transferred, A is a scaling factor, D is a constant, and B and C are the spread and offset of the sigmoid function, respectively.

CBE Device Response with Model Analyte.

To assess the capability of the nanoaperture metamaterial-based reporter to function in variable concentration chemical sensing measurements, the CBE device was assembled as shown in Figure S1, and a constant potential (in contrast to the constant current experiments described above) was applied using the Pt electrode of the analyte cell as the working electrode. In this implementation, the ITO-wire-nanoaperture metamaterial (reporter side) functioned as the CBE. To find the correct time and voltage conditions for optimum sensing, 1 mM $\text{Fe}(\text{CN})_6^{4-}$ was introduced to the analyte cell, and optical spectra were recorded at increasing time intervals. After a cumulative 5 min application of -2.0 V (Pt WE *vs.* ITO

QRCE), the sensor was nearly saturated, although some response was still obtained upon a further 2 min application - 420 s total, Figure 4(a). The normalized spectra were again expressed as a linear combination of the initial (0 s) and saturated (420 s) spectra, and the spectral progression is shown as a function of cumulative charge in Figure 4(b).

CBE Sensor Range.

Using the voltage application time required to reach near-saturation of the reporter cell at 1 mM $\text{Fe}[(\text{CN})_6]^{4-}$, further tests were conducted to examine the performance of the NSL-based reporter cell using lower concentrations of $\text{Fe}[(\text{CN})_6]^{4-}$ in the analyte cell. For these experiments, the concentration was stepped from 1 μM to 1 mM in quarter- and half-decade increments, with -2.0 V applied across the assembled CBE device for 7 min. The sensor response was observed to be below the noise floor from 1 μM to 25 μM , before increasing substantially, *viz.* Figure 5.

The limiting current for a parallel planar electrode configuration, such as the one used here, is:

$$i_{\text{lim}} = \frac{nFADC}{z} \quad (4)$$

where n = number of electrons transferred, F = Faraday constant, A = overlapping electrode area, D = diffusion coefficient, C = concentration of electroactive species, and z = electrode separation. The linearity is an obvious advantage in many kinds of experiments, but in the optical coulometry approach taken here it presents a challenge. For example, if a linear dynamic range from 1 μM to 1 mM is desired, the error in the optical readout of the nanoaperture material must be $\ll 0.1\%$, which is smaller than the noise floor observed upon optical readout of the reporter cell. If the sensing paradigm is changed such that the time is measured to achieve a desired sensor response and 1 mM is measured at 30 s, then detection of 1 μM would require more than 8 h. Obviously either scenario presents problems.

To address this conundrum, we implemented two changes. First, the noise floor which limits the measurements shown in Figure 5 was addressed through a combination of lowering the applied potential and increasing the analyte cell area. In addition, we added a series resistance to the CBE thus limiting the current at higher concentrations, designing the experiment for a constant analysis time of 1 h, rather than constant current or voltage. As shown in Table 1, a monotonic response was obtained over the analyte concentration range 100 nM – 10 μM , thus extending the viable concentration range of the CBE-enabled optical metamaterial approach. While 1 h experiment times are prohibitive, these results point the way to the proper combination of cell geometry and electrochemical driving forces to permit high sensitivity chemical sensing using the CBE-enabled metamaterials approach.

Once an experiment (or multiple experiments) is completed, the nanoaperture metamaterial may be removed from the reporter cell. Excess electrolyte may be removed via a rinse with acetone and dried under a stream of N_2 , while preserving the electrodeposited silver film and the resulting Ag-decorated nanoaperture metamaterial. This provides a physical artifact that can act as a record of the test that was performed, which is a distinct advantage over redox-

based electrochromic readouts^{23, 24} in which the reporter compound (methyl viologen) returns to a colorless state after the applied voltage bias is removed. The results of the test are easily observed visually and by imaging. Alternatively, the silver film may be removed by immersion in a wet etchant (*e.g.* Cr Etch, Sigma Aldrich) without damaging the underlying Au film, thus allowing the substrate to be re-used.

Conclusions

Post-fabrication tuning of the optical response function of metamaterials is a potentially powerful method to increase their application to a wide range of problems, specifically as demonstrated here, in chemical sensing. In this work, a large-area, tunable optical nanoaperture-based metamaterial was fabricated using scalable, inexpensive NSL. By manipulating both aperture size and spacing through easily-accessible process parameters, we demonstrated post-fabrication tuning of metamaterial optical response function and correlated the mechanism of tuning - charge transfer via electrodeposition - to a repeatable chemical sensor response. This response was leveraged by coupling the nanoaperture metamaterial to an analytical redox reaction using closed bipolar electrochemistry. The results suggest possible application of this metamaterial-based readout to point-of-care diagnostics devices, as the device configuration exhibits several distinct advantages for electrochemical biosensing and field-deployable testing. The CBE geometry physically separates the two electrochemical cells, thus minimizing cross-talk between the sensing and reporting systems and allows for remote control or detection. Further, the device can be extended to multiplex operation by combining multiple sets of analyte/reporter cell systems in parallel for simultaneous determination of several analytes. Finally, the device provides a means for electrochemical detection using a metamaterial-based optical reporter, thereby filling the sensitivity gap between fluorescent and colorimetric reporters.

Supplementary Material

Refer to Web version on PubMed Central for supplementary material.

Acknowledgements

This work was supported through a NASA Space Technology Research Fellowship (GMC, NNX16AM45H), and the Department of Energy (CO, DE FG02 07ER1585.) We thank Prof. Anthony Hoffman for the use of his optics lab and equipment. The authors also thank Irfan Khan for helpful discussions and preliminary data collection, and Galen Harden for instruction and troubleshooting of the spectrometer, and Seung-Ryong Kwon for assistance with sample fabrication and discussions concerning simulation results. Fabrication and structural characterization of the devices were performed the Notre Dame Nanofabrication Facility and the Notre Dame Integrated Imaging Facility, respectively, whose generous support is gratefully acknowledged.

References

1. Kimmel DW, LeBlanc G, Meschievitz ME and Cliffel DE, *Analyt. Chem.*, 2012, 84, 685–707. [PubMed: 22044045]
2. Turner APF, *Chem. Soc. Rev.*, 2013, 42, 3184–3196. [PubMed: 23420144]
3. Sarkar D, Liu W, Xie XJ, Anselmo AC, Mitragotri S and Banerjee K, *ACS Nano*, 2014, 8, 3992–4003. [PubMed: 24588742]
4. Li M, Shi L, Xie T, Jing C, Xiu G and Long Y-T, *ACS Sensors*, 2017, 2, 263–267. [PubMed: 28723143]

5. Ronkainen NJ, Halsall HB and Heineman WR, *Chem. Soc. Rev.*, 2010, 39, 1747–1763. [PubMed: 20419217]
6. Shao YY, Wang J, Wu H, Liu J, Aksay IA and Lin YH, *Electroanalysis*, 2010, 22, 1027–1036.
7. Kinoshita S, Yoshioka S, Fujii Y and Okamoto N, *Forma*, 2002, 17, 103–121.
8. Francesco M and Andrea A, *Chin. Phys. B*, 2014, 23, 047809.
9. Shelby RA, Smith DR and Schultz S, *Science*, 2001, 292, 77–79. [PubMed: 11292865]
10. Genet C and Ebbesen TW, *Nature*, 2007, 445, 39–46. [PubMed: 17203054]
11. Crouch GM, Han D and Bohn PW, *J. Phys. D*, 2018, 51, 193001.
12. Liu H and Lalanne P, *Nature*, 2008, 452, 728–731. [PubMed: 18401405]
13. Hennessy J, Jewell AD, Hoenk ME, Hitlin D, McClish M, Carver AG, Jones TJ and Nikzad S, *SPIE Commercial + Scientific Sensing and Imaging*, SPIE, 2017, 10209.
14. Gordon R, Sinton D, Kavanagh KL and Brolo AG, *Acc. Chem. Res.*, 2008, 41, 1049–1057. [PubMed: 18605739]
15. Yang J, Duan G and Cai W, *J. Phys. Chem. C*, 2009, 113, 3973–3977.
16. Lee SH, Bantz KC, Lindquist NC, Oh S-H and Haynes CL, *Langmuir*, 2009, 25, 13685–13693. [PubMed: 19831350]
17. Zhang X, Yonzon CR and Van Duyne RP, *J. Mater. Res.*, 2006, 21, 1083–1092.
18. Wang G, Chen X, Liu S, Wong C and Chu S, *ACS Nano*, 2016, 10, 1788–1794. [PubMed: 26760215]
19. Fosdick SE, Knust KN, Scida K and Crooks RM, *Angew. Chem. Int. Ed*, 2013, 52, 10438–10456.
20. Guerrette JP, Oja SM and Zhang B, *Analyt. Chem*, 2012, 84, 1609–1616. [PubMed: 22229756]
21. Loget G, Zigah D, Bouffier L, Sojic N and Kuhn A, *Acc. Chem. Res.*, 2013, 46, 2513–2523. [PubMed: 23719628]
22. Ulrich C, Andersson O, Nyholm L and Bjorefors F, *Angew. Chem. Int. Ed*, 2008, 47, 3034–3036.
23. Xu W, Fu K, Ma C and Bohn PW, *Analyst*, 2016, 141, 6018–6024. [PubMed: 27704078]
24. Xu W, Fu K and Bohn PW, *ACS Sensors*, 2017, 2, 1020–1026. [PubMed: 28750540]
25. Park C, Seo S, Shin H, Sarwade BD, Na J and Kim E, *Chem. Sci*, 2015, 6, 596–602. [PubMed: 28936310]
26. Masson J-F, Murray-Méthot M-P and Live LS, *Analyst*, 2010, 135, 1483–1489. [PubMed: 20358096]
27. Hu J, Fu K and Bohn PW, *Analyt. Chem*, 2018, 90, 2326–2332. [PubMed: 29260861]
28. Kim JH and Moyer PJ, *Opt. Expr*, 2006, 14, 6595–6603.
29. Zhang J, Irannejad M, Yavuz M and Cui B, *Nanoscale Research Letters*, 2015, 10, 238.
30. Rudenko A, Mauclair C, Garrelie F, Stoian R and Colombier JP, *Applied Surface Science*, 2019, 470, 228–233.
31. Irannejad M, Yavuz M and Cui B, *Photon. Res.*, 2013, 1, 154–159.
32. Silva LIB, Freitas M, Rocha-Santosa TAP and Duarte AC, *Talanta*, 2010, 82, 1403–1411. [PubMed: 20801348]

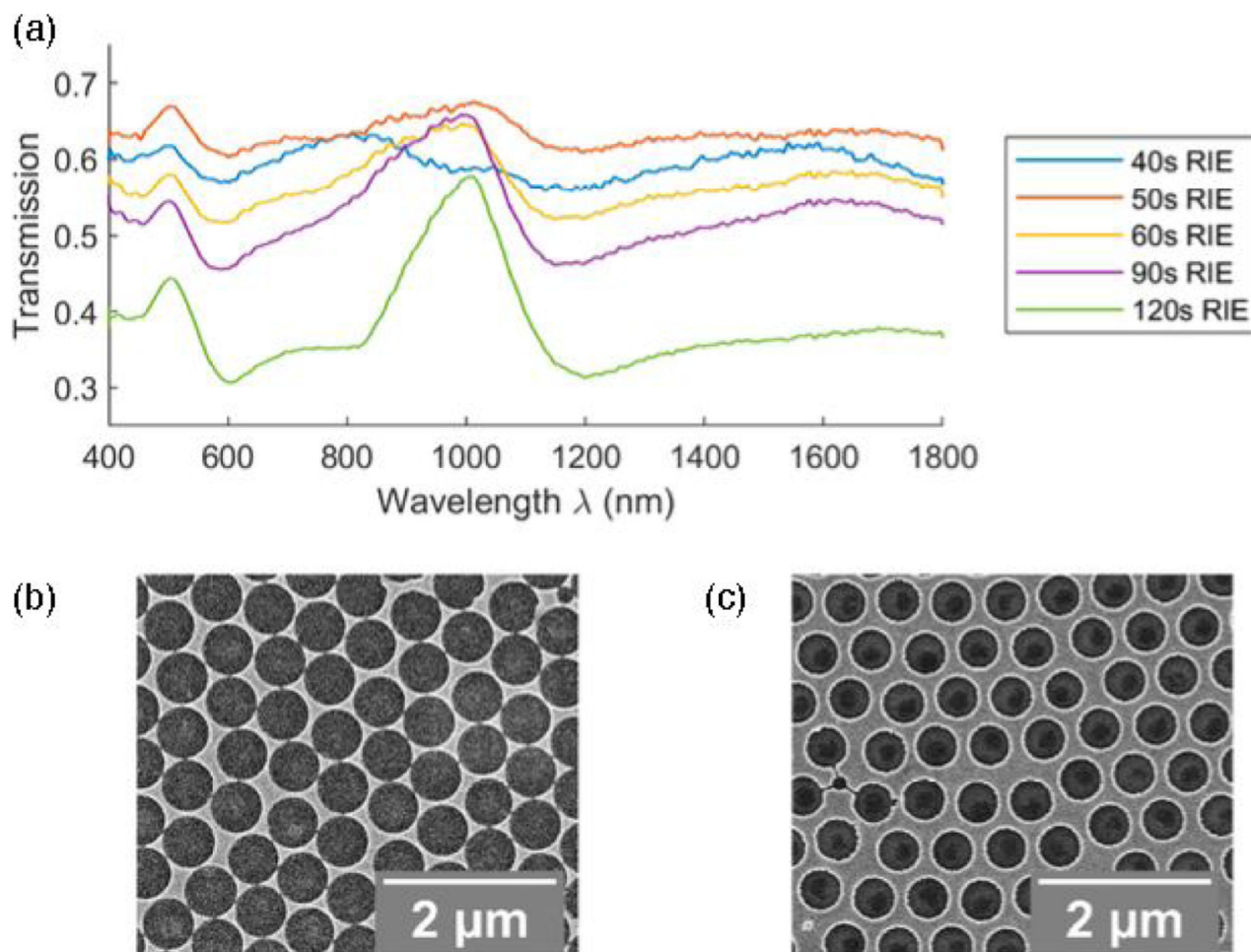


Figure 1.

(a) Optical transmission spectra of nanoaperture metamaterials obtained at 600 nm spacing using increasing O_2 plasma etch times, resulting in smaller apertures at constant center-to-center spacing. Plan view scanning-electron microscope (SEM) images of nanoaperture metamaterials obtained with (b) 30 s and (c) 2 min RIE times.

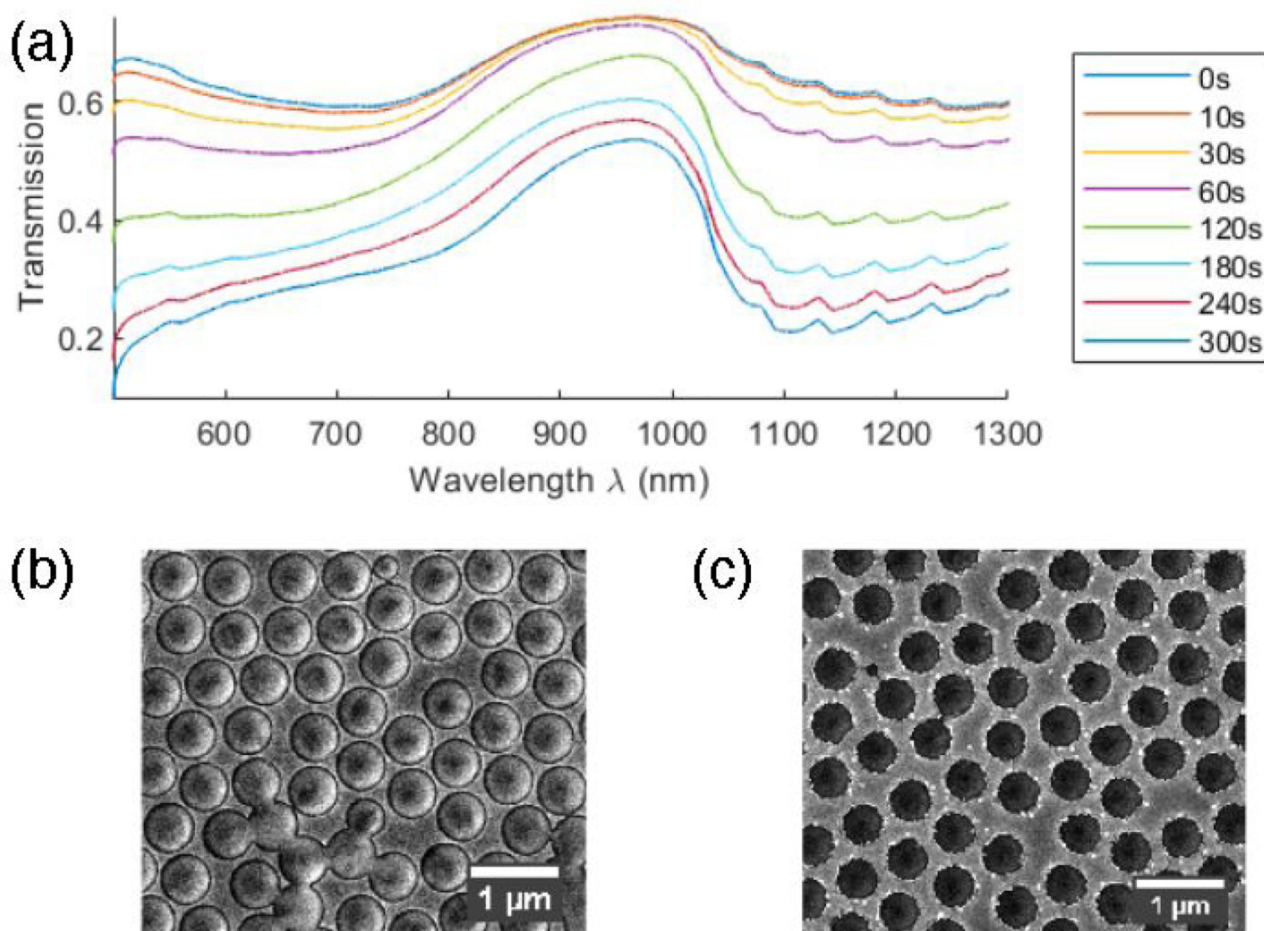


Figure 2.

(a) Transmission spectra of a nanoaperture metamaterial (600 nm spacing, 50s O_2 plasma etch) reporter cell showing post-fabrication tuning of nanoaperture metamaterial transmission spectra by galvanostatic application of 20 μA for increasing times. SEM images of the sample before (b) and after (c) showing hole shrinkage and smoothness of deposited Ag layer. EDX images are given in Figures S4 and S5 before and after deposition, respectively.

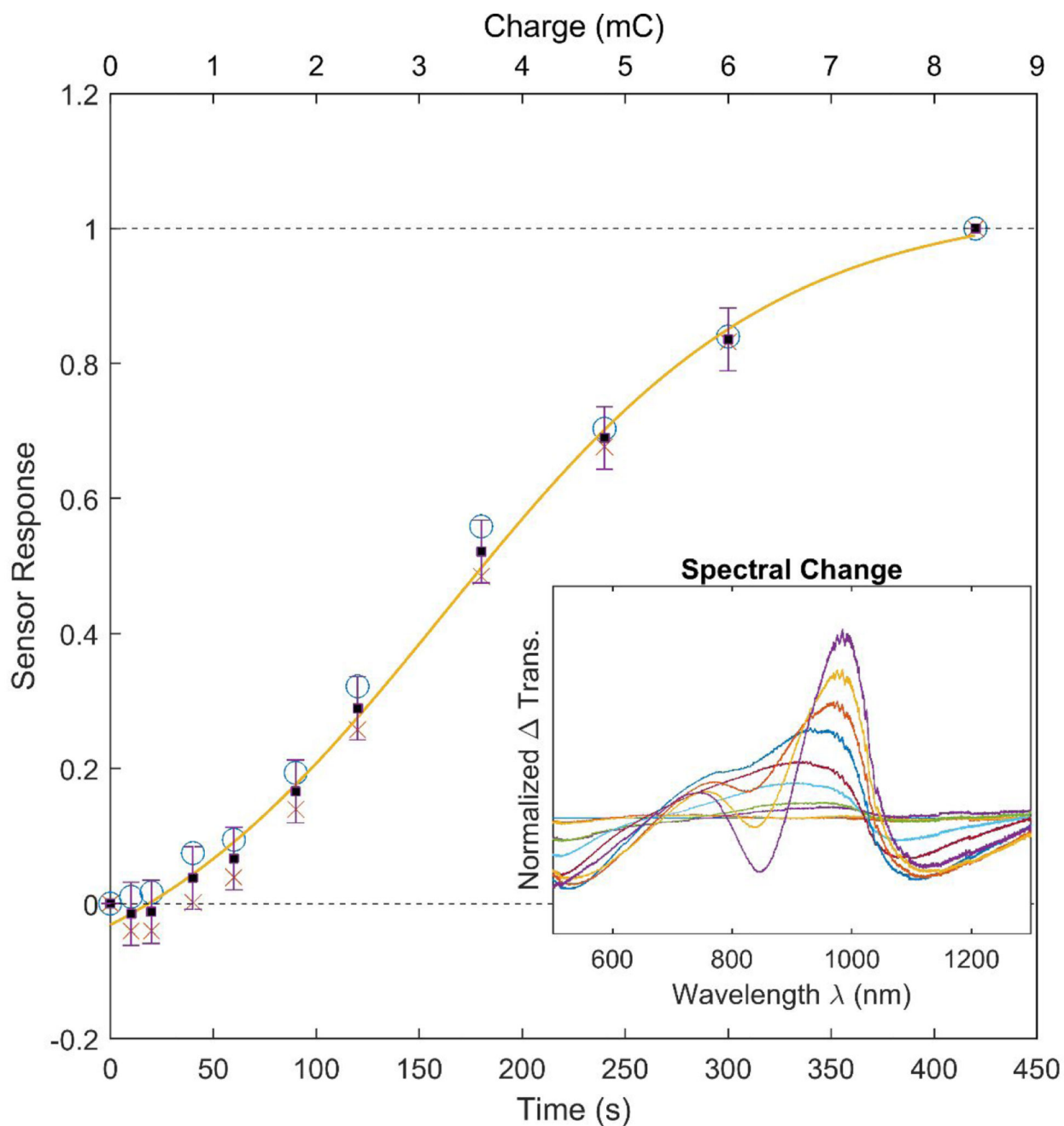


Figure 3.

Plot of sensor response vs. time during a galvanostatic deposition ($2 \mu\text{A}$) in a nanoaperture metamaterial reporter cell. Spectral response is calculated from the best-fit linear combination of starting and ending normalized spectra (x, red), while intensity response is based on the overall change in normalized transmittance (open circles, blue.) A sigmoidal response curve fit to the average of the two responses (squares, black) is given by the yellow line, with error bars $\pm 3\sigma$. (*Inset*) Normalized transmission difference (compared to the $t = 0$, $Q = 0$ spectrum) spectra.

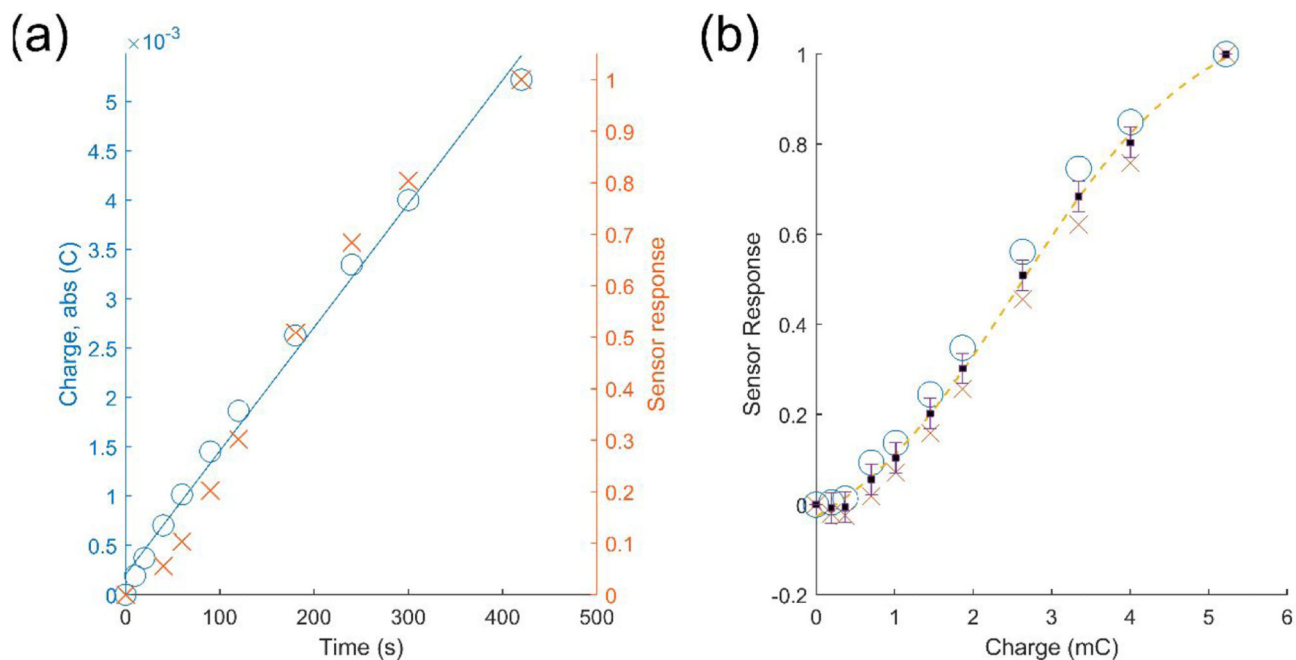


Figure 4.

CBE sensor device operation with 1 mM $\text{Fe}(\text{CN})_6^{4-}$ analyte, showing reporter cell response during constant potential application, -2.0 V Pt WE (analyte cell) vs. ITO QRCE (reporter cell), from $t = 0$ s – 420 s. (a) Charge transfer (blue circles, left axis) measured by external potentiostat, with best-fit linear regression (blue line, solid) and corresponding sensor response (red x, right axis). (b) Separate spectral response from best-fit linear combination (x, red) and intensity response corresponding to decrease in transmittance (open circles, blue) are shown as a function of the charge transfer. A sigmoidal response curve fit to the average of the two responses (squares, black) is given by the yellow line, with error bars representing $\pm 3\sigma$.

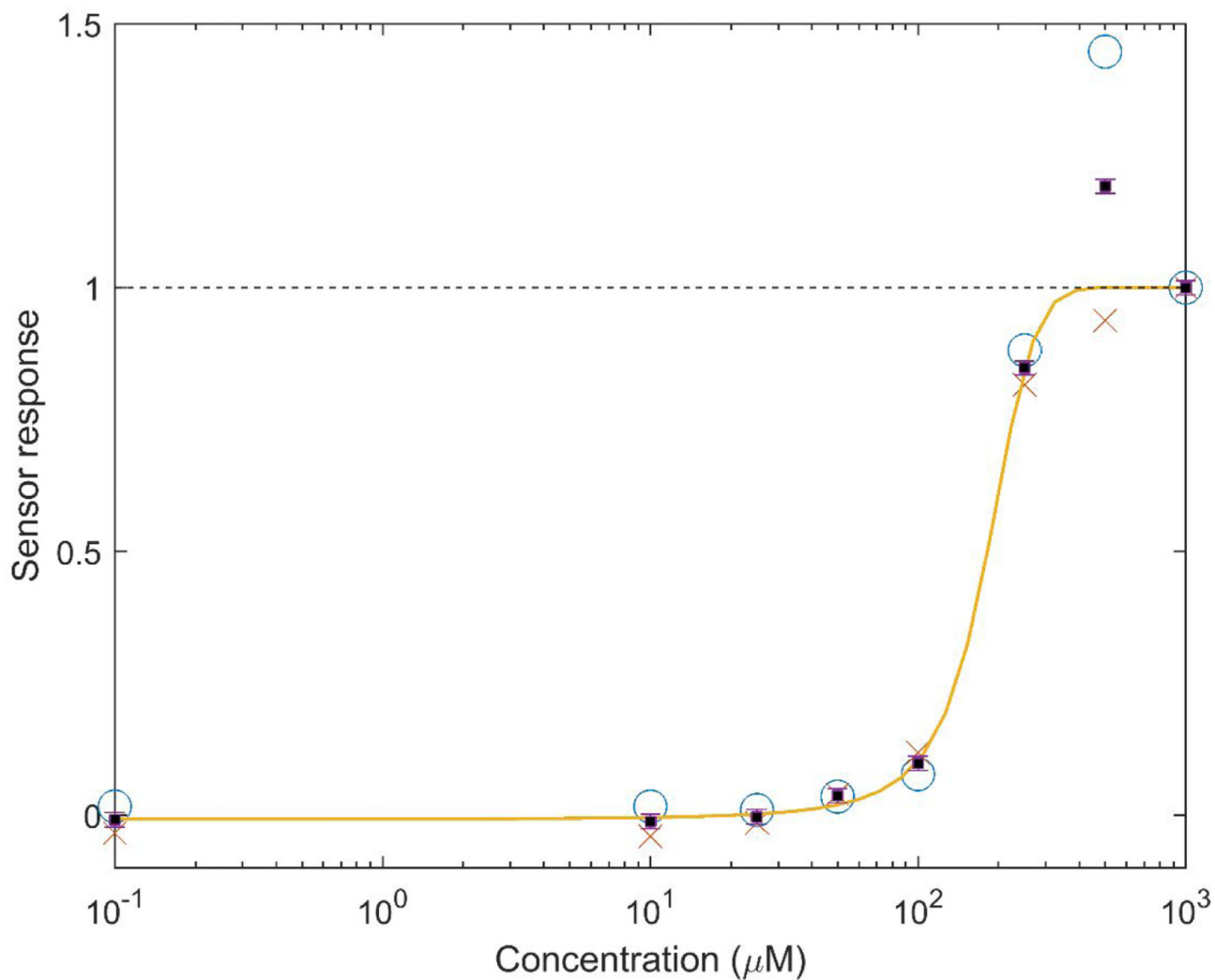


Figure 5. Proof-of-concept experiment showing sensor response as a function of concentration for $\text{Fe}[(\text{CN})_6]^{4-}$. The concentration behavior is obtained from a combined fit to the spectral (x, red) and intensity (open circles, blue) responses after application of -2.0 V vs. analyte cell Pt QRCE for 420 s. A sigmoidal response curve fit to the average of the two responses (squares, black), excluding the $500\text{ }\mu\text{M}$ outlier, is given by the yellow line, with error bars $\pm 3\sigma$ estimated from the first three concentrations.

Table 1.

Extended Range Sensor Response

Concentration	Average Sensor Response (a.u.)	Difference ^b
1 nM	-0.11	±0.11
100 nM	0.12	±0.07
1 μM	0.81	±0.07
10 μM ^a	1.00 ^a	NA ^a

^aThis concentration was used to define the saturated sensor response, S_{final} .

^bDifference between average and spectral/intensity responses.